Journal of Membrane Science Letters 6 (2026) 100123

Contents lists available at ScienceDirect

Journal of Membrane Science Letters

journal homepage: www.elsevier.com/locate/memlet

Standardizing and optimizing disk inhibition zone testing against *E. coli* for reproducible evaluation of antibacterial polymeric membranes

Mahshid Mardani [a], Mohsen Pilevar [a], Nima Behzadnia [a], Shemai'ya Peak [b], Mona Bavarian [c], Siamak Nejati [c], Mark Elliott [a,*], Mostafa Dadashi Firouzjaei [a,*]

[a] Department of Civil, Construction, and Environmental Engineering, University of Alabama, Tuscaloosa, AL, 35487, USA
[b] Department of Chemical and Biological Engineering, University of Alabama, Tuscaloosa, AL, 35487, USA
[c] Department of Chemical and Biomolecular Engineering, The University of Nebraska-Lincoln, Lincoln, NE, 68588-8286, United States

ARTICLE INFO

Keywords:
Antibacterial membranes
Standardization
Biofouling control
AgMOF
PHMB

ABSTRACT

The disk inhibition zone test is a widely used and visually interpretable method for evaluating the antibacterial properties of membranes. However, the lack of a consistent, standardized methodology for disk inhibition zone testing limits reliable assessment of antibacterial performance in membranes. Herein, we introduce a systematic and reproducible framework for investigating the key experimental parameters, including bacterial concentration (10^5–10^9 CFU/mL), nutrient media (i.e., tryptic soy broth (TSB)) concentration (15–60 g/L), incubation time (6–10 h), and various bacterial spreading techniques such as overlayer (OL), glass spreader (GS), and cotton swab (CS) method. Quantitative image analysis in ImageJ, combined with comprehensive statistical evaluation, revealed that bacterial concentration and TSB levels were the most influential factors in determining inhibition zone diameter. In contrast, the choice of spreading technique significantly affected the uniformity and integrity of the inhibition zone. Results showed that utilizing a bacterial concentration of 10^7 CFU/mL, TSB concentration of $\geq$ 30 g/L, incubation times of 8-10 h, and the overlayer (OL) method, although less commonly used in the literature, led to the most consistent inhibition zones, as these conditions promote stable bacterial growth kinetics and uniform lawn formation. This framework provides a reliable approach to standardize antibacterial membrane testing and improve cross-study comparability and validation.

1. Introduction

Membrane technologies play a critical role in desalination (Karki et al., 2024), wastewater reuse (Shehata et al., 2023), potable water protection (Ghofrani et al., 2023), and sustainable water treatment (Ćurić et al., 2021). Membranes act as selective barriers that rely on size exclusion to block contaminants while allowing clean water to pass (Zandi et al., 2025). However, biological fouling (biofouling) remains a major challenge, leading to reduced water flux (Sun et al., 2020), higher energy consumption (Zou et al., 2016), and shortened membrane lifespan (Zhang et al., 2014).

To mitigate biofouling, various antimicrobial agents, such as polymers (Bryaskova et al., 2025), biocidal nanomaterials like metal-based nanoparticles (NPs) (Firouzjaei et al., 2018), carbon-based materials (Martinez et al., 2016), MXene (Firouzjaei et al., 2025; Seidi et al., 2023), and metal-organic frameworks (Zirehpour et al., 2016) have been incorporated into membrane structures to inhibit bacterial growth and biofilm formation (Dadashi Firouzjaei et al., 2024; Firouzjaei et al., 2025; Li et al., 2018; Lin et al., 2025; Liu et al., 2024; Pilevar et al., 2025). Various experimental methods have been utilized to assess the antibacterial efficacy of modified membranes, including colony-forming unit (CFU) counting (Alkahtani et al., 2023), suspension or adhesion methods (Bento de Carvalho et al., 2024; Hall et al., 2020), biofilm assays (Hall et al., 2020), and disk inhibition zone tests (Cunliffe et al., 2021). Among these, the disk inhibition zone test is widely used due to its simplicity and cost-effectiveness (Hudzicki, 2009), where a membrane sample is placed on an inoculated agar plate (AATCC, T. 2017), and the resulting clear zone is used to assess antibacterial activity (Åhman et al., 2019).

However, experimental parameters such as bacterial concentration, nutrient media composition, incubation time, and spreading technique can significantly affect inhibition zone results for antibacterial membranes, making comparisons across studies difficult (Hamouda et al., 2021; Yan et al., 2023; Zan et al., 2023). As summarized in Table S1,

* Corresponding authors.
E-mail addresses: melliott@eng.ua.edu (M. Elliott), mdfirouzjaei@crimson.ua.edu (M. Dadashi Firouzjaei).

https://doi.org/10.1016/j.memlet.2026.100123
Received 23 June 2026; Received in revised form 13 July 2026; Accepted 14 July 2026
Available online 14 July 2026

variations in testing conditions across antibacterial membrane studies make direct comparisons of inhibition zone results difficult. Therefore, a systematic evaluation of these factors is needed to improve test reliability, reproducibility, and comparability.

In this study, a standardized and reproducible framework for disk inhibition zone testing of antibacterial membranes is developed. Key experimental parameters, including spreading technique, bacterial concentration, incubation time, nutrient media concentration, and membrane type, are systematically evaluated. Statistical analysis is used to quantify their influence on inhibition zone diameter and quality. This framework provides a practical method for consistently and comparably assessing antibacterial membranes.

2. Experimental methods

Disk inhibition zone tests were performed using *Escherichia coli (E. coli)* at concentrations of 10^5–10^9 CFU/mL on TSB agar plates containing 15, 30, and 60 g/L. Based on the preparation instructions for BD Difco™ TSB (Becton 2026), 30 g/L was used as the standard full-strength concentration, while 15 and 60 g/L were selected to represent half-strength and double-strength TSB, respectively. Before testing, bacterial cultures were grown to the log phase and then transferred to PBS. Three spreading techniques were evaluated: overlayer (OL), glass spreader (GS), and cotton swab (CS) (Table S2). Membrane samples with a diameter of 1.5 cm were placed with their active/coated surfaces facing downward in direct contact with the inoculated agar surface or, for the OL method, the inoculated soft agar overlayer. The plates were incubated at 37 °C for 6, 8, and 10 h. Polyhexamethylene biguanide (PHMB) is a cationic polymer due to its protonated biguanide groups (Sowlati-Hashjin et al., 2020; Wang et al., 2021), whereas AgMOF-containing membranes can display negative surface-charge properties, partly because of deprotonated carboxylate groups in the BTC ligand (Firouzjaei et al., 2018; Seyedpour et al., 2020). Accordingly, negatively charged antibacterial membranes (NCAMs) were created by depositing AgMOF particles onto PVDF microfiltration membranes via dead-end filtration, while positively charged antibacterial membranes (PCAMs) were produced by modifying PVDF membranes with PHMB. These membranes were used as representative antibacterial membranes with different surface charges and antibacterial mechanisms. Details of membrane preparation and characterization are provided in Figures S1 and S3, respectively. Inhibition zone diameters were measured using ImageJ (Figure S2). In addition to diameter, circularity was measured from the area and perimeter of each inhibition zone to support the classification of defective and non-defective zones (Table SD1). Each experimental condition was tested in triplicate using independent agar plates and membrane coupons. Statistical analysis was performed using JMP Pro 17 with regression models to evaluate the effects of experimental parameters.

3. Results and discussion

3.1. Effects of bacterial concentration on disk inhibition zone

Fig. 1 presents a comparative analysis of inhibition zones formed at different bacterial concentrations. The box plots in Fig. 1a_1, b_1, and c_1 show the distribution of inhibition zone diameters, with colors indicating defective and non-defective zones (Table SD2). Representative agar plate images (Fig. 1a_2–a_6, b_2–b_6, and c_2–c_6) further illustrate the visual differences in zone formation under fixed TSB concentration (30 g/L) and incubation time (8 h).

Bacterial concentration had a limited effect on the average inhibition zone diameter, which ranged from 19 to 22 mm across all spreading techniques (Fig. 1a_1, b_1, and c_1). A slight reduction in zone diameter was observed at higher bacterial concentrations (≥ 10^8 CFU/mL),

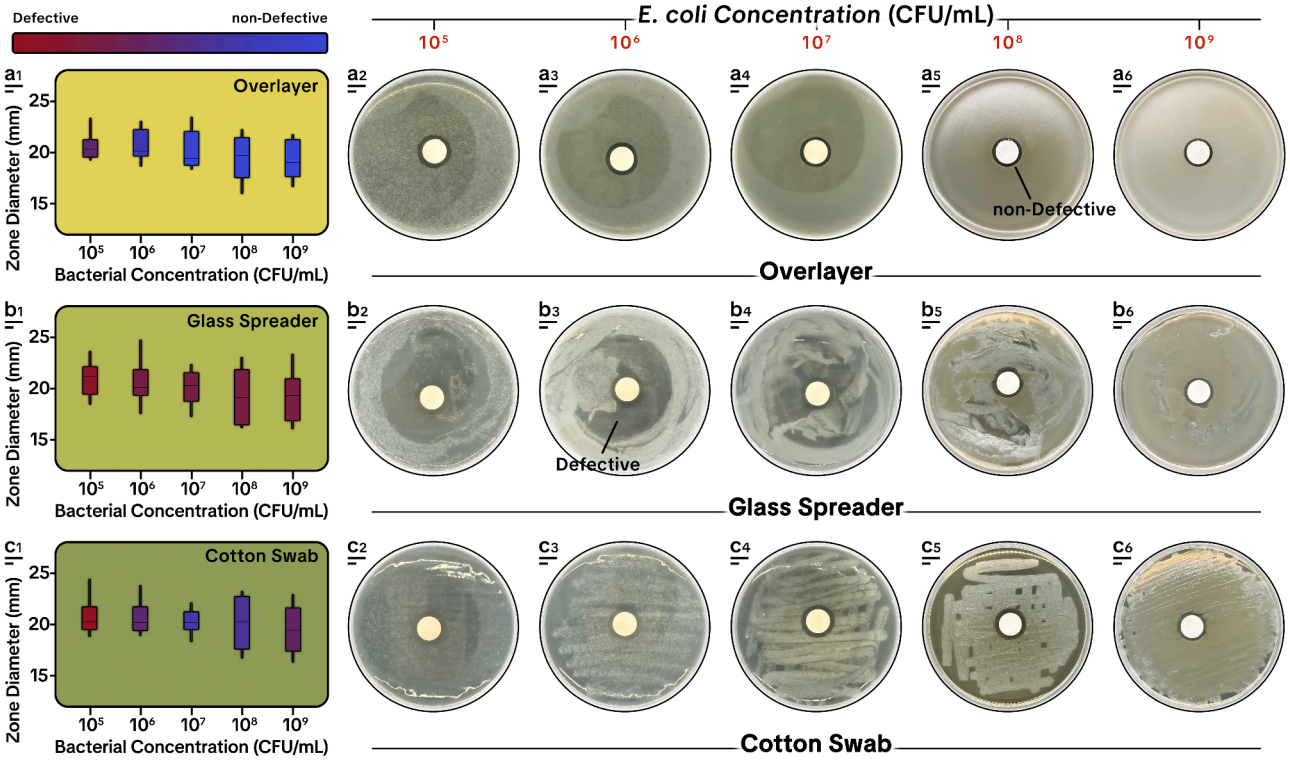

Fig. 1. Disk inhibition zone results of NCAM using three spreading techniques: **(a_1)** OL, **(b_1)** GS, and **(c_1)** CS. evaluated at *E. coli* at five concentrations (10^5, 10^6, 10^7, 10^8, and 10^9 CFU/mL). Box plots show zone diameters, while images **($a_{2–6}$, $b_{2–6}$, and $c_{2–6}$)** illustrate inhibition zones after 8 h incubation on TSB agar (30 g/L). Bacterial concentration significantly affected the inhibition zone diameter, as indicated by the regression model ($F = 25.27$, $p < 0.0001$). Box colors summarize the defect status among the three replicates: blue represents 0/3 defective zones, blue-purple represents 1/3, red-purple represents 2/3, and red represents 3/3 defective zones, as defined in Table SD2. The colors are independent of inhibition-zone diameter and circularity.

particularly for the GS method. The greater defectiveness observed at 10^8 CFU/mL with the CS method was likely due to uneven manual spreading rather than to bacterial concentration, since the OL method produced uniform zones under the same conditions. In contrast, bacterial concentration strongly affected zone quality. At lower bacterial concentrations of 10^5 and 10^6 CFU/mL, defective inhibition zones were frequently observed, particularly with the GS (Fig. 1$b_{2,3}$) and CS techniques (Fig. 1$c_{2,3}$). This behavior was attributed to delayed bacterial growth and incomplete lawn formation, which resulted in uneven clearing and irregular inhibition patterns (Qiu et al., 2022; Rewak-Soroczynska et al., 2022). In contrast, higher bacterial concentrations, especially 10^9 CFU/mL, often resulted in bacterial overgrowth and possible masking of membrane-derived antibacterial activity (Pimentel et al., 2020). Overall, the intermediate concentration of 10^7 CFU/mL produced a more uniform bacterial lawn and non-defective inhibition zones with the CS and OL methods. In contrast, nonuniform lawns and defective zones were common with the GS method at all concentrations (Figure S5).

Among all techniques, the OL method consistently produced the most uniform and non-defective inhibition zones across the tested concentration range (Figure S6). This behavior can be attributed to the soft agar environment, which promotes homogeneous bacterial dispersion and stable growth conditions. In contrast, manual surface-spreading methods, including GS and CS, can introduce uneven cell distribution, surface disruption, and localized drying, thereby compromising lawn uniformity and zone integrity (Meng et al., 2021). Glass-bead spreading is also based on mechanical movement across the agar surface and may therefore be subject to operator-dependent variability similar to the GS technique. The uniformity of bacterial distribution can depend on factors such as the number of beads, the direction and intensity of plate movement, and the spreading time (Prusokiene et al., 2021; Sanders, 2012). Circularity analysis further supported this finding, showing that OL produced more circular and uniform zones, while GS and CS often showed lower circularity due to irregular or defective zone formation (Table SD1). These results indicate that bacterial concentration and spreading technique must be controlled to avoid a misleading interpretation of antibacterial membrane performance.

3.2. Effects of incubation time on disk inhibition zones

Figs. 2 and S8 show the effect of incubation time on inhibition zone diameter and defectiveness across the three spreading techniques. Minimal changes in average zone diameter were observed from 6 to 10 h, with values remaining around 19–21 mm regardless of spreading technique (Fig. 2a–c), indicating that incubation time did not significantly affect zone diameter (Table S3). However, incubation time strongly influenced zone quality and the reliability of visual interpretation.

The short incubation time (6 h) resulted in numerous defective inhibition zones in the GS and CS techniques (Fig. 2d), particularly at lower bacterial concentrations (10^5 and 10^6 CFU/mL), where incomplete lawn formation was evident (Fig. 2d). These observations indicate that lower bacterial concentrations require a longer incubation period to form a continuous bacterial lawn and clearly define the inhibition zone boundary. Higher bacterial concentrations led to visible lawns forming more rapidly, although excessive growth at the highest concentration could partially mask the inhibition zone. In contrast, the OL method produced more uniform zones at short incubation times, particularly at bacterial concentrations ($\geq 10^7$ CFU/mL). This behavior is attributed to the semi-solid and moist soft agar layer, which promotes uniform bacterial dispersion and faster lawn development (Be'er et al., 2009; Schwarcz et al., 2016). In contrast, GS and CS showed delayed zone development (Fig. 2d), likely due to uneven bacterial distribution, localized drying, and mechanical disturbance during manual spreading (Ohgiwari et al., 1992).

Increasing the incubation time to 8–10 h reduced the number of defective zones and produced clearer inhibition boundaries (Figs. 2a and S7). The OL method produced predominantly non-defective zones after 8–10 h, whereas GS and CS still showed some defective zones due to inconsistencies in manual spreading. These results indicate that incubation time must be sufficient to allow bacterial lawn development and antimicrobial diffusion without overgrowth. Therefore, an incubation time of 8–10 h provides a more reliable window for evaluating membrane-derived antibacterial activity (Mai et al., 2025).

The time-lapse video (Video S1) further confirmed the role of incubation time in the development of the inhibition zone. Bacterial growth initiated within the first hour, and a noticeable color change of the NCAM was observed after approximately 2 h, likely associated with Ag^0 oxidation and Ag^+release (Berchel et al., 2011; Jaros et al., 2020). The inhibition zone became faintly visible between 5.5 and 6 h and progressively expanded into a stable, circular, and non-defective zone by 8 h. These observations support the conclusion that sufficient incubation time is required for both bacterial lawn development and antimicrobial diffusion, making 8–10 h a reliable window for reproducible inhibition zone evaluation. Key stages of zone development are shown in Figure S9.

3.3. Effects of TSB agar composition on disk inhibition zones

The effects of TSB concentration on disk inhibition zone formation were evaluated using TSB agar plates prepared at three concentrations (15, 30, and 60 g/L). Fig. 3 shows the distribution, variability, and defectiveness of inhibition zones across different TSB and bacterial concentrations, with additional representative plate images shown in Figure S11. A relatively low TSB concentration of 15 g/L resulted in a large number of defective inhibition zones across all three spreading techniques, particularly with the CS method (Fig. 3c), due to delayed bacterial growth (Rewak-Soroczynska et al., 2022). Low nutrient availability can restrict bacterial metabolism, slow replication, and reduce motility, leading to poor lawn development and irregular colony patterns (Wang et al., 2023). Increasing the TSB concentration levels to 30 and 60 g/L led to fewer defective zones in the OL and CS (Figs. 3a-c and S10) techniques.

As demonstrated in Figs. 3a–c, increasing TSB concentration from 15 to 60 g/L resulted in larger inhibition zone diameters across all spreading techniques, highlighting the significant influence of nutrient concentration on zone formation. Although higher TSB concentrations generally produced larger inhibition zones (~23 mm), this trend does not fully align with previous studies (; Brady and Katz, 1990; Okada et al., 2007). While inhibition zone diameter is commonly attributed to bacterial species, inoculum density, and nutrient concentration, these factors alone cannot fully explain the observed variability. For example, *E. coli* grown in different media, such as TSB and Mueller–Hinton (MH), exhibits distinct metabolic behavior. This difference has been linked to the higher peptide and glucose content in TSB, which accelerates bacterial metabolism, whereas MH is designed to minimize variability in diffusion-based measurements (Ratiu et al., 2017). In addition, variations in inhibition zone diameter have been reported under similar biological conditions when different membrane substrates were used, suggesting that membrane-specific properties contribute (Dahms and Hellio, 2009).

3.4. Effects of membrane surface charge on disk inhibition zones

Surface charge is another membrane-specific factor influencing inhibition zone formation. Gram-negative bacteria such as *E. coli* have negatively charged cell surfaces due to phosphate and carboxyl groups, which can affect their interactions with charged membranes and antimicrobial agents (Abbaszadegan et al., 2015; Ratiu et al., 2017). Positively charged materials can enhance antibacterial activity through stronger electrostatic interactions with bacterial membranes (Simcock et al., 2020).

To further evaluate this effect, the role of membrane surface charge

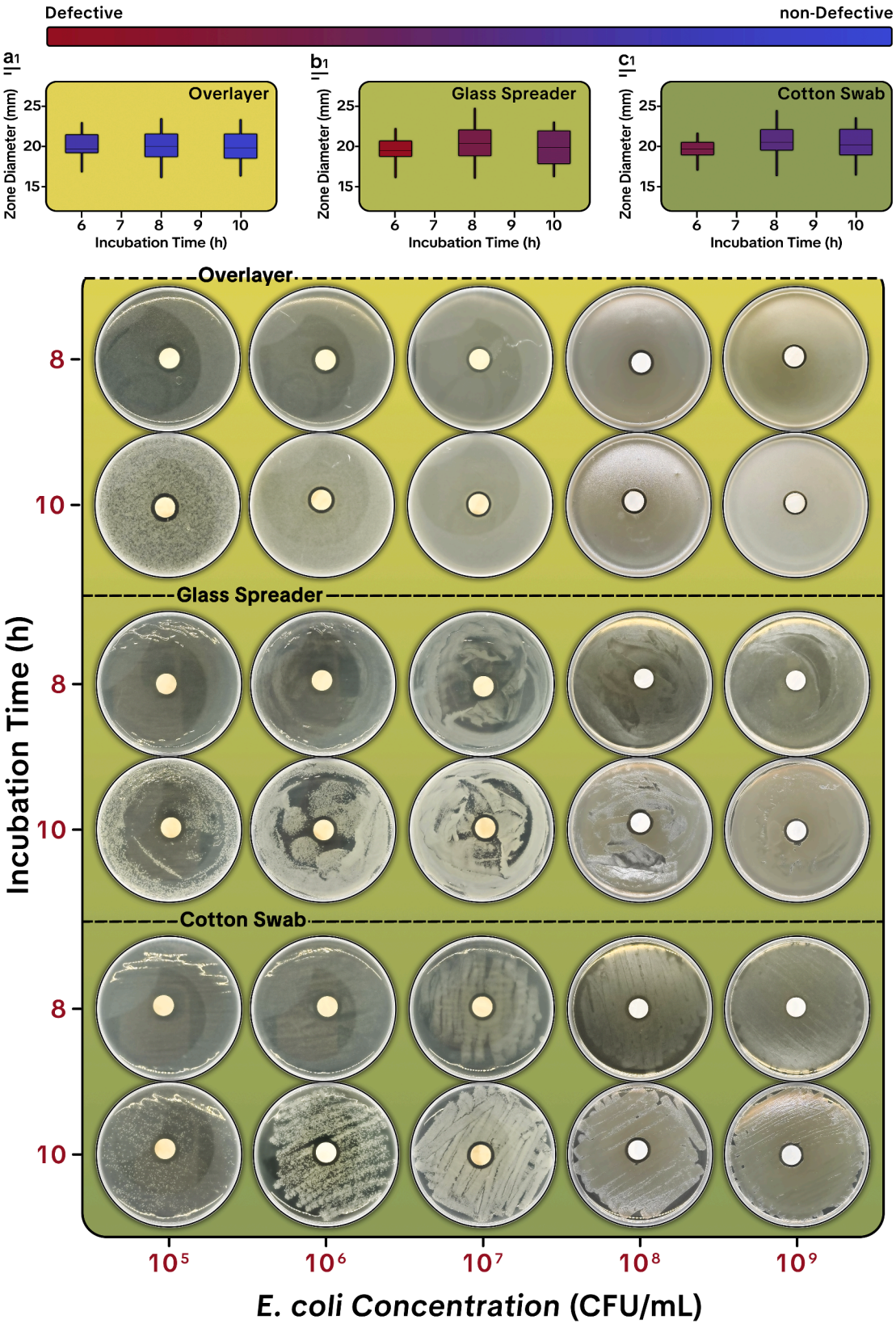

Fig. 2. Effect of incubation time on disk inhibition-zone formation for NCAM using three spreading techniques: **(a)** overlayer (OL), **(b)** glass spreader (GS), and **(c)** cotton swab (CS). **(d)** Representative photographs of the inhibition zones. Box plots show the distribution of inhibition-zone diameters, while box colors summarize replicate defect status according to Table SD2. Incubation time did not significantly affect inhibition-zone diameter in the regression model ($F = 1.75$, $p = 0.1877$). However, increasing the incubation time from 6 to 8–10 h improved zone quality and reduced defective-zone formation, particularly for the GS and CS methods.

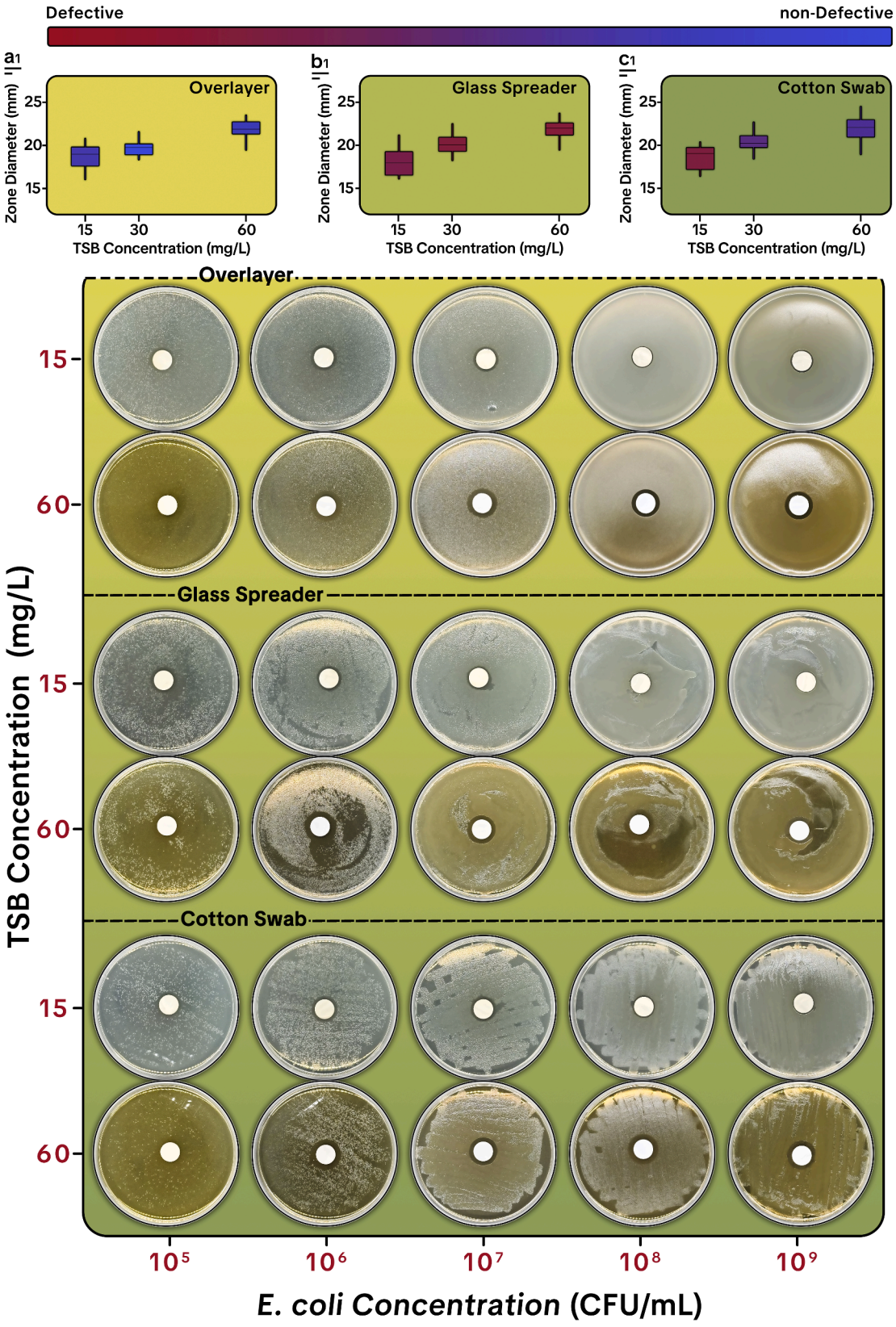

Fig. 3. Effect of TSB concentration on disk inhibition zone formation across different bacterial spreading techniques and *E. coli* concentrations. Diagrams **(a)** OL, **(b)** GS, and **(c)** CS techniques. (**d**) Representative photographs show inhibition-zone formation under the tested conditions. Box colors summarize the defect status of the three replicates, as defined in Table SD2. Statistical analysis identified TSB concentration as the most significant factor affecting inhibition-zone diameter in the regression model ($F = 254.54$, $p < 0.0001$).

was investigated using a PCAM based on PHMB (Kathuria et al., 2021; Liang et al., 2020) and an NCAM based on AgMOF (Pilevar et al., 2025), which were tested under controlled conditions using the OL method and 10^7 CFU/mL *E. coli* across different TSB concentrations and incubation times (Fig. 4). For PCAM, the measured clear-zone diameter decreased as TSB concentration increased, with the largest value observed at 15 g/L, whereas NCAM produced larger inhibition zones at 30 and 60 g/L TSB (Fig. 4b_1, c). These trends suggest that inhibition zone formation depends not only on bacterial growth conditions but also on membrane surface chemistry and antibacterial mechanism (Sowlati-Hashjin et al., 2020; Yamada et al., 2010). PHMB exhibits antibacterial activity mainly through electrostatic interactions with negatively charged bacterial cell surfaces (Hornschuh et al., 2020; Vaz et al., 2023). The clear region corresponding to the PCAM surface is consistent with contact-mediated antibacterial activity, while the peripheral halo may indicate limited desorption and diffusion of PHMB into the agar. In contrast, the NCAM inhibition halo is associated with the release and diffusion of antibacterial silver species (Sánchez et al., 2022). These results demonstrate that inhibition zone formation depends on both the testing conditions and the membrane's antibacterial mechanism. Therefore, the comparison between PCAM and NCAM confirms that the optimized testing conditions are relevant to different antibacterial membrane chemistries rather than a single membrane system.

3.5. Statistical analysis

The least squares regression model showed good agreement between predicted and experimental inhibition zone diameters (Figure S12a), with R-squared (R^2) and root mean square error (RMSE) values of 0.72 and 0.99, respectively. ANOVA confirmed the model's statistical significance (p-value < 0.05), indicating that at least one factor significantly affects the inhibition zone diameter (Table S4). The model reliability was further supported by the normal distribution of residuals (Figure S12b) and the absence of outliers in the studentized residual plot (Figure S12c).

The statistically significant variables were identified at a 95% confidence level ($\alpha = 0.05$), indicating their substantial influence on the disk inhibition zone diameter (Table S3). Notably, TSB concentration was identified as the most significant factor influencing zone diameter (Table S3), consistent with the trends observed in Fig. 3. Bacterial concentration was the second most significant factor, followed by the interactions between TSB concentration and bacterial concentration and between TSB concentration and incubation time. A reduced model was also developed by removing non-significant terms (see Table S6), and additional statistical details are provided in Table S5. Nominal logistic regression confirmed the model's statistical significance for defective/non-defective zone formation (p-value < 0.0001), with an overall prediction accuracy of 77.8%. The confusion matrix showed higher prediction accuracy for defective zones than for non-defective zones (Table S7). Effect likelihood ratio analysis further identified the spreading technique as the most influential factor affecting defective/non-defective zone formation, followed by bacterial concentration and incubation time (Table S8).

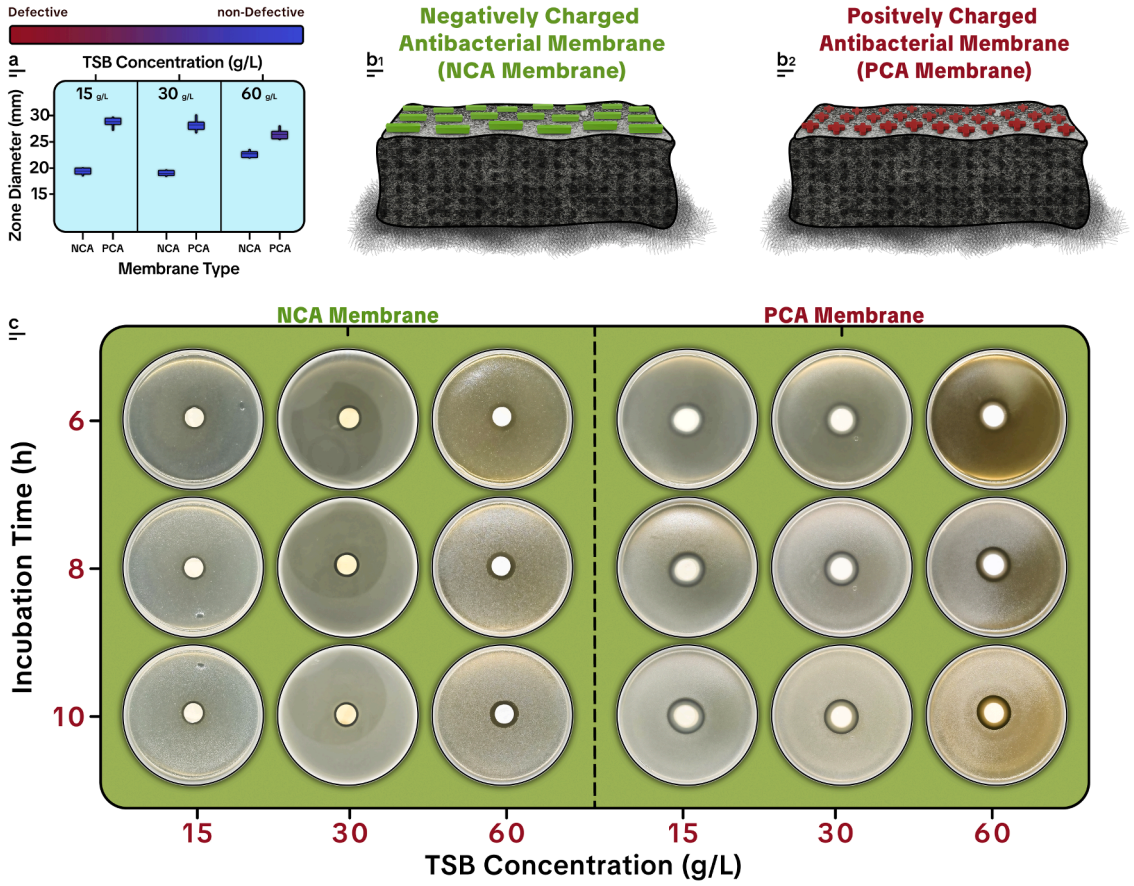

Fig. 4. Disk inhibition analysis of NCAM and PCAM under different TSB concentrations and incubation times. **(a)** Measured clear-zone diameters for NCAM and PCAM at TSB concentrations of 15, 30, and 60 g/L. All experiments were performed using the OL technique with an *E. coli* concentration of 10^7 CFU/mL. Schematic illustrations show the surface characteristics of **(b_1)** the AgMOF-based NCAM and **(b_2)** the PHMB-modified PCAM. **(c)** Representative images obtained after 6, 8, and 10 h of incubation. The PCAM exhibited a distinct region at the membrane surface, and in some cases, a peripheral halo. This suggests mainly contact-mediated PHMB activity with possible limited PHMB desorption and diffusion.

4. Conclusion

A systematic framework for disk inhibition zone testing was established to enhance the reliability and reproducibility of antibacterial membrane evaluations. The results demonstrated that experimental conditions significantly influenced inhibition-zone formation, with TSB concentration mainly affecting zone diameter and spreading technique strongly impacting zone quality. Bacterial concentration and incubation time also impacted the uniformity and stability of bacterial lawn formation. Since uniform bacterial lawn formation is essential for clearly identifying the inhibition zone boundary, the required incubation time may vary depending on the bacterial species and initial bacterial concentration. Among the tested methods, the OL technique produced the most uniform, well-defined, and reproducible inhibition zones by dispersing *E. coli* within soft agar before applying it to the TSB agar plate. Although absolute inhibition-zone diameters may vary with bacterial species, membrane properties, and antibacterial mechanisms, the proposed framework provides consistent testing conditions that reduce false-positive zones and enable more reliable comparisons of antibacterial membranes.

CRediT authorship contribution statement

Mahshid Mardani: Writing – original draft, Investigation, Formal analysis, Conceptualization. **Mohsen Pilevar:** Writing – review & editing, Formal analysis. **Nima Behzadnia:** Investigation. **Shemai'ya Peak:** Investigation. **Mona Bavarian:** Writing – review & editing, Validation, Resources. **Siamak Nejati:** Writing – review & editing, Validation. **Mark Elliott:** Writing – review & editing, Supervision, Resources, Methodology, Conceptualization. **Mostafa Dadashi Firouzjaei:** Writing – review & editing, Visualization, Validation, Resources, Project administration, Methodology, Conceptualization.

Declaration of competing interest

The authors declare that they have no known competing financial interests or personal relationships that could have appeared to influence the work reported in this article.

Supplementary materials

Supplementary material associated with this article can be found, in the online version, at doi:10.1016/j.memlet.2026.100123.

Data availability

Data will be made available on request.

References

AATCC, T., 2017. Test Method for Antifungal Activity, Assessment on Textile Materials: Mildew and Rot Resistance of Textile Materials. American Association of Textile Chemists and Colorists, Durham, NC, USA.

Abbaszadegan, A., et al., 2015. The effect of charge at the surface of silver nanoparticles on antimicrobial activity against gram-positive and gram-negative bacteria: a preliminary study. J. Nanomater. 2015 (1), 720654.

Åhman, J., Matuschek, E., Kahlmeter, G., 2019. The quality of antimicrobial discs from nine manufacturers—EUCAST evaluations in 2014 and 2017. Clin. Microbiol. Infect. 25 (3), 346–352.

Alkahtani, S., Al-Johani, N.S., Alarifi, S., 2023. Mechanistic insights, treatment paradigms, and clinical progress in neurological disorders: current and future prospects. Int. J. Mol. Sci. 24 (2), 1340.

Becton, Dickinson and Company, 2026. Available from: https://www.bd.com/en-us/products-and-solutions/products/product-families/dehydrated-culture-media-and-additives?utm.

Be'er, A., et al., 2009. Paenibacillus dendritiformis bacterial colony growth depends on surfactant but not on bacterial motion. J. Bacteriol. 191 (18), 5758–5764.

Bento de Carvalho, T., Barbosa, J.B., Teixeira, P., 2024. Assessing antimicrobial efficacy on plastics and other non-porous surfaces: a closer look at studies using the ISO 22196: 2011 standard. Biology 13 (1), 59.

Berchel, M., et al., 2011. A silver-based metal–organic framework material as a 'reservoir' of bactericidal metal ions. New J. Chem. 35 (5), 1000–1003.

Brady, M.S., Katz, S.E., 1990. Factors influencing optimization of diffusion assays for antibiotics. J. Assoc. Off. Anal. Chem. 73 (2), 202–205.

Bryaskova, R., et al., 2025. Innovative Antibacterial Polymer Coatings. Appl. Sci. 15 (4), 1780.

Cunliffe, A.J., et al., 2021. How do we determine the efficacy of an antibacterial surface? A review of standardised antibacterial material testing methods. Antibiotics 10 (9), 1069.

Ćurić, I., Dolar, D., Karadakić, K., 2021. Textile wastewater reusability in knitted fabric washing process using UF membrane technology. J. Clean. Prod. 299, 126899.

Dadashi Firouzjaei, M., et al., 2024. Functionality review and life cycle assessment of a silver-based MOF for advanced material and sustainability applications. Graphene 2D Mater. 1–18.

Dahms, H.-U., Hellio, C., 2009. Laboratory bioassays for screening marine antifouling compounds. Adv. Mar. Antifouling Coat. Technol. 275–307.

Firouzjaei, M.D., et al., 2018. A novel nanocomposite with superior antibacterial activity: a silver-based metal organic framework embellished with graphene oxide. Adv. Mater. Interface. 5 (11), 1701365.

Firouzjaei, M.D., et al., 2018. Exploiting synergetic effects of graphene oxide and a silver-based metal–organic framework to enhance antifouling and anti-biofouling properties of thin-film nanocomposite membranes. ACS Appl. Mater. Interface. 10 (49), 42967–42978.

Firouzjaei, M.D., et al., 2025. A perspective on MXene-enhanced biofiltration-membrane water reuse treatment systems: a review and experimental validation. Desalination 593, 118198.

Ghofrani, B., et al., 2023. Fabrication and characterization of novel PES-based nanocomposite hollow fiber membranes for the hemodialysis process. Sep. Purif. Technol. 317, 123939.

Hall, T.J., et al., 2020. A call for action to the biomaterial community to tackle antimicrobial resistance. Biomater. Sci. 8 (18), 4951–4974.

Hamouda, H., Abdel-Ghafar, H., Mahmoud, M., 2021. Multi-walled carbon nanotubes decorated with silver nanoparticles for antimicrobial applications. J. Environ. Chem. Eng. 9 (2), 105034.

Hornschuh, M., et al., 2020. In vitro evaluation of contact-active antibacterial efficacy of Ti-Al-V alloys coated with the antimicrobial agent PHMB. Acta Biomater. 106, 376–386.

Hudzicki, J., 2009. Kirby-Bauer disk diffusion susceptibility test protocol. Am. Soc. Microbiol. 15 (1), 1–23.

Jaros, S.W., et al., 2020. Antiviral, antibacterial, antifungal, and cytotoxic silver (I) BioMOF assembled from 1, 3, 5-triaza-7-phoshaadamantane and pyromellitic acid. Molecules 25 (9), 2119.

Karki, S., et al., 2024. Polymeric membranes for industrial applications: recent progress, challenges and perspectives. Desalination 573, 117200.

Kathuria, D., et al., 2021. Biguanides: Species with versatile therapeutic applications. Eur. J. Med. Chem. 219, 113378.

Li, Y., et al., 2018. Impact of anti-biofouling surface coatings on the properties of nanomaterials and their biomedical applications. J. Mater. Chem. B 6 (1), 9–24.

Liang, A., et al., 2020. Porous poly (hexamethylene biguanide) hydrochloride loaded silk fibroin sponges with antibacterial function. Materials 13 (2), 285.

Lin, Q., et al., 2025. Electrostatically enhanced surface segregation boosts anti-fouling performance of mixed matrix membranes. J. Membr. Sci. 725, 124036.

Liu, S., et al., 2024. Performance improvement and application of copper-based nanomaterials in membrane technology for water treatment: a review. J. Environ. Manag. 370, 122755.

Mai, Z., et al., 2025. Effects of different feeding strategies for the frozen Antarctic krill meal on growth, muscle nutrition, digestive enzyme activity, immunity, molting, and gut microbiota structure of Cherax quadricarinatus. Front. Mar. Sci. 12, 1573152.

Martinez, Z.S., et al., 2016. Fullerene derivatives strongly inhibit HIV-1 replication by affecting virus maturation without impairing protease activity. Antimicrob. Agents Chemother. 60 (10), 5731–5741.

Meng, L., et al., 2021. The effect of bacterial functional characteristics on the spread of antibiotic resistance genes in expanded granular sludge bed reactor treating the antibiotic wastewater. Ecotoxicol. Environ. Saf. 225, 112714.

Ohgiwari, M., Matsushita, M., Matsuyama, T., 1992. Morphological changes in growth phenomena of bacterial colony patterns. J. Phys. Soc. Jpn. 61 (3), 816–822.

Okada, A., et al., 2007. Targeting two-component signal transduction: a novel drug discovery system. Methods in Enzymology. Elsevier, pp. 386–395.

Pilevar, M., et al., 2025. Analysis of metal–organic framework and polyamide interfaces in membranes for water treatment and antibacterial applications. Small Methods 9 (4), 2401566.

Pimentel, M., et al., 2020. ACG clinical guideline: small intestinal bacterial overgrowth. Off. J. Am. Coll. Gastroenterol. ACG 115 (2), 165–178.

Prusokiene, A., et al., 2021. Effectiveness of glass beads for plating cell cultures. Phys. Rev. E 103 (5), 052410.

Qiu, Y., et al., 2022. The effects of ventilation, humidity, and temperature on bacterial growth and bacterial genera distribution. Int. J. Environ. Res. Public Health 19 (22), 15345.

Ratiu, I.-A., et al., 2017. The effect of growth medium on an *Escherichia coli* pathway mirrored into GC/MS profiles. J. Breath Res. 11 (3), 036012.

Rewak-Soroczynska, J., et al., 2022. Culture media composition influences the antibacterial effect of silver, cupric, and zinc ions against Pseudomonas aeruginosa. Biomolecules 12 (7), 963.

Sánchez, A., et al., 2022. Antimicrobial properties of amino-acid-derived N-heterocyclic carbene silver complexes. Pharmaceutics 14 (4), 748.

Sanders, E.R., 2012. Aseptic laboratory techniques: plating methods. J. Vis. Exp. (63), 3064.
Schwarcz, D., et al., 2016. Uniform modeling of bacterial colony patterns with varying nutrient and substrate. Phys. D. 318, 91–99.
Seidi, F., et al., 2023. MXenes antibacterial properties and applications: a review and perspective. Small 19 (14), 2206716.
Seyedpour, S.F., et al., 2020. Toward sustainable tackling of biofouling implications and improved performance of TFC FO membranes modified by Ag-MOF nanorods. ACS Appl. Mater. Interface. 12 (34), 38285–38298.
Shehata, N., et al., 2023. Membrane-based water and wastewater treatment technologies: issues, current trends, challenges, and role in achieving sustainable development goals, and circular economy. Chemosphere 320, 137993.
Simcock, P.W., et al., 2020. Modified bacterial lipids which alter membrane surface charge reduce binding of antimicrobial peptides. BioRxiv, p. 2020.04. 24.057349.
Sowlati-Hashjin, S., Carbone, P., Karttunen, M., 2020. Insights into the polyhexamethylene biguanide (PHMB) mechanism of action on bacterial membrane and DNA: a molecular dynamics study. J. Phys. Chem. B 124 (22), 4487–4497.
Sun, Z., et al., 2020. High water permeating thin film composite polyamide nanofiltration membranes showing thermal responsive gating properties. J. Water Process Eng. 36, 101355.
Vaz, L.M., et al., 2023. Sterilized polyhexanide-releasing chitosan membranes with potential for use in antimicrobial wound dressings. Membranes 13 (11), 877.
Wang, J., et al., 2021. Fabrication of a dual-action membrane with both antibacterial and anticoagulant properties via cationic polyelectrolyte-induced phase separation. ACS Appl. Mater. Interfaces 13 (13), 14938–14950.
Wang, J., et al., 2023. Simulation of various biofilm fractal morphologies by agent-based model. Colloids Surf. B 227, 113352.
Yamada, H., et al., 2010. Direct observation and analysis of bacterial growth on an antimicrobial surface. Appl. Environ. Microbiol. 76 (16), 5409–5414.
Yan, G., et al., 2023. Antibacterial biodegradable nanofibrous membranes by hybrid needleless electrospinning for high-efficiency particulate matter removal. Chem. Eng. J. 461, 142137.
Zan, J., et al., 2023. Hyaluronic acid encapsulated silver metal organic framework for the construction of a slow-controlled bifunctional nanostructure: Antibacterial and anti-inflammatory in intrauterine adhesion repair. Int. J. Biol. Macromol. 230, 123361.
Zandi, Z., et al., 2025. Electro-conductive silver-coated polyamide-imide membranes for sustainable water treatment. Adv. Sustain. Syst., e00527
Zhang, Q., et al., 2014. Characterization of biofouling in a lab-scale forward osmosis membrane bioreactor (FOMBR). Water Res. 58, 141–151.
Zirehpour, A., et al., 2016. The impact of MOF feasibility to improve the desalination performance and antifouling properties of FO membranes. RSC Adv. 6 (74), 70174–70185.
Zou, S., et al., 2016. Energy Consumption By recirculation: a Missing Parameter When Evaluating Forward Osmosis. ACS Publications.